Surfaces of intermetallic compounds: An *ab initio* DFT study for B20-type AlPd

M. Krajčí[1] and J. Hafner[2]

[1]*Institute of Physics, Slovak Academy of Sciences, Dúbravská cesta 9, SK-84511 Bratislava, Slovak Republic*

[2]*Fakultät für Physik and Center for Computational Materials Science, Universität Wien, Sensengasse 8/12, A-1090 Wien, Austria*

(Received 24 August 2012; published 30 January 2013)

The low-index surfaces of the AlPd compound crystallizing in the B20 (FeSi-type) structure have been investigated using *ab initio* density functional methods. The space group of the B20 structure is $P2_13$, with four threefold rotational axes along the ⟨111⟩ directions and three twofold screw axes along the ⟨100⟩ directions, but no inversion symmetry. The B20 structure exists in two enantiomorphic forms related by inversion. The termination of the structure perpendicular to the twofold screw axes is uniquely defined: The corrugated {100} surfaces are formed by the characteristic zigzag Al-Pd chains separated by shallow troughs. Perpendicular to the ⟨210⟩ directions the structure consists of slightly puckered planes containing Al and Pd in equal numbers. The {210} surfaces shows pseudo-fivefold symmetry. Their structure is shown to be closely related to that of the {110} surfaces of the B2 structure. Both the {100} and {210} surfaces undergo some structural relaxation, but no reconstruction changing their (1×1) periodicity. While perpendicular to the ⟨100⟩ and ⟨210⟩ directions only one surface termination is possible, perpendicular to the threefold ⟨111⟩ directions there are several possible surface terminations differing in structure and chemical composition. Because of the lack of inversion symmetry the threefold {111} surfaces have polar character. The (111) and $(\bar{1}\bar{1}\bar{1})$ surfaces are not equivalent; the (111) surfaces of one enantiomorph are identical to the $(\bar{1}\bar{1}\bar{1})$ surfaces of the other form (and vice versa). In both the (111) and $(\bar{1}\bar{1}\bar{1})$ directions several surface terminations are possible. The formation of threefold surfaces has been studied by simulated cleavage experiments and by calculations of the surface energies of all possible terminations. Perpendicular to the ⟨111⟩ direction the lowest energy has been found for a bilayer with three Al atoms per surface cell in the upper layer and one Al and one Pd in the lower part. The preferable termination perpendicular to the $\langle\bar{1}\bar{1}\bar{1}\rangle$ direction is more symmetric; it consists again of a bilayer with three Al atoms in the upper and three Pd atoms in the lower part. The surface energy of this termination further decreases if the Pd triplet is covered by additional Al atom. The calculated surface energies permit us to perform a Wulff construction of the equilibrium shape of AlPd crystallites. {100} and {210} facets together occupy 77% of the surface area in about equal proportion. The high anisotropy of the energy of the {111} surfaces results in the substantial difference of the surface areas of the opposite threefold facets.

DOI: 10.1103/PhysRevB.87.035436 PACS number(s): 68.35.bd, 68.35.Md, 73.20.At

I. INTRODUCTION

While the low-index surfaces of simple close-packed metals have been studied for decades and are today well understood,[1] the surfaces of complex intermetallic compounds represent a largely unexplored area worthy of fundamental research. In a complex crystal structure many inequivalent atomic planes with different structure and chemical composition may exist perpendicular to a given crystallographic direction. From the known crystal structure it is generally very difficult to predict the preferable cleavage planes and which atomic planes are exposed at the surface. Because of possible structural relaxations or reconstructions of the surface, as well as desorption processes, the structure and stoichiometry of the crystal surfaces can differ from those of the corresponding atomic layers in the bulk. The task of the determination of the stable surfaces is further complicated by the number of crystallographic directions that have to be considered. The determination of the stability and atomistic structure of the surfaces of a complex intermetallic compound can be thus a difficult and challenging task.

The surfaces of complex intermetallic compounds exhibit physical and chemical properties interesting for technical applications. In contrast to the surfaces of substitutional alloys where the distribution of the different species is more or less random, the chemical order on the surfaces of intermetallic compounds is well defined and periodically repeated. These surfaces can be used as substrates for the deposition of atomic or molecular thin films or as templates for growing various nanostructures.[2,3] Recently intermetallic compounds formed by transition metals (TMs) and simple metals have attracted much interest as efficient and highly selective catalysts and it has been argued that the isolation and periodic distribution of the active sites on their surfaces plays a very important role.[4] However, while the surfaces of simple close-packed TMs have only a few inequivalent reaction sites, the surfaces of complex TM intermetallics provide a rich variety of different adsorption sites, leading to a multitude of possible reaction channels for catalytic reactions.

During the last years significant progress has been realized in the experimental preparation and characterization of surfaces of complex metallic compounds.[5–8] Quasicrystals and their periodic approximants have attracted particular attention as a special class of metallic compounds with a very high structural complexity. It is remarkable that despite their complex aperiodic atomic structure the surfaces of some Al-TM quasicrystals are atomically flat. Surfaces of stable quasicrystals such as the fivefold surface of icosahedral Al-Pd-Mn or the tenfold surface of decagonal Al-Co-Ni have been studied intensively both by experimental[9–11] and *ab inito* theoretical methods.[12–15]

In this field the interplay between experimental investigations and theoretical modeling is particularly important. A standard experimental method for surface investigations is scanning tunneling microscopy (STM). High-resolution STM images provide information about the structure of the surface at a nanometer scale. To achieve an understanding the structure at the atomic scale it is necessary to compare experimental STM images with simulated images for several tentative structural models of the surface based on *ab initio* DFT (density functional theory) methods.[12–15] Another important experimental method for quantitative surface structure analysis is low-energy electron diffraction (LEED), which is sensitive to several layers below the surface and able to provide important information about relaxation or reconstruction of surface and subsurface layers. As the method is based on fitting experimental data in a parameter space derived from tentative structural models, additional information on appropriate structural models from DFT calculations is very essential.[8]

Structural modeling based on the DFT methods has proven to be very useful because it provides also information not directly accessible to experiment. For a prediction of the positions of the preferred cleavage planes a simulation of the cleavage process and its interpretation in terms of the chemical bonding in the material is very helpful. The calculation of the energies of competing surfaces permits the prediction of the equilibrium shape of crystallites and the determination of the surfaces areas occupied by different facets.

In our recent work[15] we have studied the $\{100\}$ surfaces of orthorhombic $Al_{13}Co_4$ which is an approximant to the decagonal Al-Ni-Co quasicrystal and exhibits interesting catalytic activity for acetylene hydrogenation.[16–19] In the present work we investigate the surfaces of the AlPd compound crystalizing in the B20 structure. The motivation of our study is threefold: (i) As we shall demonstrate in detail below the B20 structure is closely related to that of the intensively studied icosahedral Al-Pd-Mn quasicrystal. The picture of chemical bonding in the simpler periodic compound is helpful for understanding that in the more complex quasicrystal, the properties of some of the low-index surfaces of the B20 are related to those of the quasicrystalline surfaces. (ii) The AlPd compound is isostructural and isoelectronic to GaPd. Both GaPd and AlPd have been identified as selective catalysts for the partial hydrogenation of alkynes.[4,19–22] In our recent works on AlPd and GaPd as catalysts for the hydrogenation of acetylene to ethylene[23,24] we have concentrated our investigations on the $\{210\}$ surface which was found to be highly reactive and to provide excellent selectivity. It is remarkable that in both types of intermetallic catalysts (orthorhombic $Al_{13}Co_4$ and B20-type AlPd and GaPd) the catalytically active surfaces are those with pseudo-fivefold symmetry.[17,23,24] (iii) While the work described here was already in progress Rosenthal *et al.*[25] presented an investigation of the polar $(\bar{1}\bar{1}\bar{1})$ surfaces of GaPd using x-ray and ultraviolet photoelectron spectroscopy (XPS, UPS), STM, LEED, and thermal desorption spectroscopy (TDS) of adsorbed CO. LEED and STM indicate a smooth, bulk truncated surface with a (1×1) unit cell. TDS shows that different surface terminations are found on surfaces prepared at different temperatures. For a high preparation temperature of 870 K a termination with only a single Pd atom per unit cell in the top layer has been suggested. A denser termination seems to dominate at lower preparation temperature, but it is still an open question whether this surface is Ga or Pd terminated.

Our paper is organized as follows. In Sec. II we present the methodology and some details on structural models and computational cells. In Sec. III we summarize the calculated structural data of AlPd and we describe the B20 structure in terms of a tiling of two kinds of rhombohedra, establishing the correlation with the structure of icosahedral quasicrystals. We present a picture of the at least partially covalent bonding determining the details of the B20 structure which is also important for the interpretation of the stability of the surfaces. In Secs. IV A and IV B we study structural properties of $\{100\}$ and $\{210\}$ surfaces, respectively. We demonstrate that the $\{210\}$ surface shows a (pseudo-)fivefold symmetry similar to that of the fivefold surface of the quasicrystal. We also show that this surface of the B20 structure plays the same role as the $\{110\}$ surfaces of the B2 (CsCl) structure. As the polar threefold (111) and $(\bar{1}\bar{1}\bar{1})$ surfaces are not identical their investigation in Sec. IV C is much more complicated. While perpendicular to the $\langle 100\rangle$ and $\langle 210\rangle$ directions only one surface termination is possible, perpendicular to the threefold $\langle 111\rangle$ directions there are several possible surface terminations differing in structure and chemical composition. We have calculated the equilibrium structures and surface energies of all possible terminations. In Sec. V the surface energies are used in a Wulff construction of the equilibrium shape of AlPd crystallites. It is found that the twofold $\{100\}$ and the pseudo-fivefold $\{210\}$ surfaces occupy nearly 80% of the surface area. Anisotropy of the $\{111\}$ and $\{\bar{1}\bar{1}\bar{1}\}$ facets is analyzed.

II. COMPUTATIONAL METHOD AND STRUCTURAL MODELS

Electronic structure calculations have been performed using the Vienna *Ab initio* Simulation Package (VASP).[26,27] VASP produces an iterative solution of the Kohn-Sham equations of density functional theory (DFT) within a plane-wave basis. We used the semilocal exchange-correlation functional in the generalized gradient approximation (GGA) proposed by Perdew *et al.*[28] The basis set contains plane waves with a kinetic energy up to $E_{\text{cutoff}} = 600$ eV. The self-consistency iterations were stopped when total energies are converged to within 10^{-6} eV.

For each surface termination we have constructed a structural model in the form of a slab cut from the bulk structure. Periodically repeated slabs are separated by a vacuum layer of 14 Å. The atomic structure of the surfaces has been optimized by static relaxations using a quasi-Newton method and the Hellmann-Feynman forces acting on the atoms. For the twofold $\{100\}$ and the pseudo-fivefold $\{210\}$ surfaces one can construct a symmetric slab where top and bottom surfaces are identical. Because of their polar character this is not possible for the $\{111\}$ surfaces; here all slabs have different surfaces at top and bottom. The thickness of the slabs should be large enough to represent the bulk structure in the central part and to stabilize the surface. For calculations of the surface energies we have used slabs with a thickness of $\approx$16–20 Å consisting of 10 (for $\{210\}$ surfaces) to 18 (for

{111} surfaces) atomic layers. The lateral dimensions of the computational cells for the twofold (010) and pseudo-fivefold (120) surfaces are equal to the dimensions of one elementary surface cell. For the threefold (111) and $(\bar{1}\bar{1}\bar{1})$ surfaces we use orthorhombic computational cells containing two rhombic surface cells. The surface area $x \times y$ of the computational cell for the AlPd(120) surface is 10.984 Å × 4.912 Å. The size of the computational cell in the z direction is 33.95 Å. Surface energies were calculated using a $4 \times 8 \times 1$ k-point mesh for Brillouin-zone integration. Calculations for other surfaces were performed with similar accuracy.

III. B20 CRYSTAL STRUCTURE

Many compounds crystallize in the B20 (FeSi) structure. In addition to Si- (CrSi, MnSi, FeSi, and CoSi) and Ge-based compounds (CrGe, MnGe, FeGe, and CoGe), intermetallic compounds with Al (AlPd, AlPt) and Ga (GaPd, GaPt) are reported.[29] The B20 structure is thus preferentially formed by polyvalent elements with a stronger (Si, Ge) or weaker (Al, Ga) covalent character with transition metals at equiatomic composition. The reason why these elements adopt the complex low-symmetry B20 structure instead of the simpler B1 (NaCl) or B2 (CsCl) structure with high symmetry is in the covalent character of the interatomic bonding described in more detail below.

The B20 (FeSi-type) structure has space group $P2_13$ (No. 198). The Bravais lattice is simple cubic, but the overall point symmetry is tetrahedral. The space group consists of four threefold rotational axes oriented along the ⟨111⟩ directions and three twofold screw 2_1 axes consisting of a 180° rotation around a cubic axis, followed by a nonprimitive translation by $(\frac{1}{2},\frac{1}{2},0)$ and combinations thereof. The B20 structure has 8 atoms per elementary cell; the Pearson symbol is cP8. In FeSi both Fe and Si are located at Wyckoff positions ($4a$) with coordinates (u,u,u), $(u+0.5,0.5-u,-u)$, $(-u,0.5+u,0.5-u)$, and $(0.5-u,-u,0.5+u)$ and $u(\mathrm{Fe}) = 0.137$ and $u(\mathrm{Si}) = 0.842$. The point symmetry of the Fe and Si sites is a threefold rotation C_3. Because of the lack of inversion symmetry the B20 structure exists in two enantiomorphic forms labeled by Gille *et al.*[30] as A and B. The coordinates (x,y,z) of atoms are related to those in the other by an inversion operation $(-x,-y,-z)$. Energetically both forms are equivalent. The structural data presented in Table I correspond to the A form.

In the AlPd compound Al atoms occupy Si sites and Fe is replaced by Pd. The values of calculated and experimental internal coordinates are collected in Table I. The B20 (FeSi) structure may be considered as derived from the B1 (NaCl) structure. If in the B20 setting the internal parameter u is equal to $u(\mathrm{Fe}) = 0.25$ and $u(\mathrm{Si}) = 1 - u(\mathrm{Fe}) = 0.75$, the B20 structure is identical to the B1 structure. The transformation B1→B20 induces rather large displacements of the Fe and Si atoms. The space-group symmetry is reduced from $Fm\bar{3}m$ to $P2_13$.

TABLE I. Calculated lattice constant a and internal coordinates u for considered B20 structures, compared to experiment.

System		a (Å)	Internal coordinates u			
FeSi	theor.	4.453	Si	0.840	Fe	0.136
	exp. Ref. 29	4.489	Si	0.842	Fe	0.137
AlPd	theor.	4.902	Al	0.844	Pd	0.147
	exp. Ref. 29	4.859	Al	0.847	Pd	0.143
Ideal B20				0.8455		0.1545
Ammann				0.905		0.955
B1(NaCl)				0.75		0.25

An interesting view of the B20 structure in terms of an "ideal B20" structure was proposed by Vočadlo *et al.*[31] They recognized that for $u(\mathrm{Fe}) = 1/(4\tau) = 0.1545$ and $u(\mathrm{Si}) = 1 - 1/(4\tau) = 0.8455$ [where $\tau = (1+\sqrt{5})/2$ is the golden mean] each atom has exactly seven nearest neighbors of the opposite kind at a distance of $a\sqrt{3}/(2\tau)$. Note (see Table I) that the positions of the atoms in AlPd are very close to the ideal ones. The seven nearest neighbors occupy seven of the twenty vertices of a pentagonal dodecahedron centered at the atom. This arrangement of the coordinating atoms led Dmitrienko[32] to interpret the B20 structure as a low-order crystalline approximant to an icosahedral Al-TM quasicrystal (e.g., i-Al-Pd-Mn). The atomic structure of a quasicrystal can be obtained by the projection method.[33] The quasiperiodicity of an icosahedral quasicrystal is closely related to the golden mean τ. A method to construct periodic approximants to the infinite quasicrystal consists of replacing this irrational number in the projection method by a fraction of two subsequent Fibonacci numbers. This creates a sequence of periodic structures with increasing size of the elementary cell. The B2 and B20 structures are the lowest-order approximants in this sequence. The B20 structure is thus a first step in complexity from the B2 structure toward the structure of the Al-TM (F-type) quasicrystals.

The icosahedral point group of the quasicrystal is very useful for understanding the nature of the interatomic bonding in the B20 structure. In the ideal B20 structure the nearest-neighbor bonds are oriented along the threefold symmetry axes of the icosahedral point group. The icosahedral point group has 20 threefold rotational axes. To distinguish these icosahedral threefold symmetry directions from the cubic threefold directions we shall refer to the icosahedral threefold directions in the B20 structure as the pseudo-threefold directions. As already noted the interatomic bonds along the pseudo-threefold directions have covalent character.

As the B20 structure has a very low point-group symmetry it is rather difficult to visualize it. The building principle of the B20 structure can be interpreted in terms of a tiling of prolate and oblate rhombohedra with an edge length e related to the cubic lattice constant a by $e = a\sqrt{3}/(2\tau)$. Along each Cartesian direction the B20 structure consists of a sequence of alternating prolate and oblate rhombohedra; see Fig. 1. The elementary cell contains four prolate and four oblate rhombohedra. The edges of the rhombohedra are oriented along the pseudo-threefold directions. The only pseudo-threefold directions that coincide with the cubic threefold directions are the short diagonals of the oblate rhombohedra (the dashed lines in Fig. 1). Each atom has seven neighbors of the opposite chemical type, six nearest-neighbor bonds coincide with the edges of the tiling, the seventh with the body diagonal of the oblate rhombohedron.

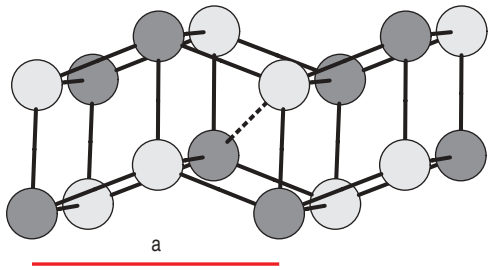

FIG. 1. (Color online) The structure of B20 can be interpreted as a packing of prolate and oblate rhombohedra. In each Cartesian direction the B20 structure is formed by a sequence of alternating prolate and oblate rhombohedra (with dashed diagonal). The length of the lattice constant a is marked explicitly (red line segment). The elementary cell consists of 4 prolate and 4 oblate rhombohedra.

We note that the rhombohedra of the ideal B20 structure are different from the Ammann (or golden) rhombohedra (sometimes called also the 3D Penrose tiles). While in the ideal B20 structure the parameter u is $u = 1/(4\tau)$ and the edges are oriented along the threefold symmetry axes (yellow sticks in the well-known Zometool construction kit[34]), in the "golden" B20 structure built by Ammann rhombohedra the value of the internal parameter u is $u = 1/(4\tau^2)$ and the edges are oriented along the fivefold symmetry axes (it is built from red sticks of the Zometool construction kit[34]).

The relation of the ideal B20 structure to the icosahedral quasicrystals can also be seen through the concept of the canonical cells introduced by Henley.[35] The ideal B20 structure is a canonical cell tiling consisting of 24 A cells, 8 B cells, and 8 C cells. If the threefold edges in the B20 structure are replaced by golden prolate rhombohedra and the nearest-neighbor bonds along the twofold axes (blue sticks[34]) are replaced by golden rhombic dodecahedra one gets a $2/1$ approximant to the F-type icosahedral quasicrystal. The $1/1$ approximant to the quasicrystal can be constructed by applying the same procedure to the B2 structure. The size of the Penrose tiles in this quasicrystalline approximant is related to the size of the canonical cells by the factor τ^3. One can thus recognize the ideal B20 structure as a $0/1$ approximant in the hierarchy of approximants to the F-type icosahedral quasicrystal.

A. Electronic structure and covalent character of interatomic bonding

A peculiar feature of the electronic spectrum of FeSi and of many isoelectronic compounds is a narrow band gap in the Fe-d-Si-p bands at the Fermi energy. In AlPd with one electron more per formula unit the gap is reduced to a pseudogap located about 1 eV below the Fermi energy. The conditions for the formation of a band gap in FeSi-type compounds and in the structurally related quasicrystals have been discussed in detail by Krajčí and Hafner.[36] Gap formation is closely related to the crystal structure and the topology of the bands. In the undistorted B1 structure where the bonds form straight chains along the Cartesian axes with equal interatomic distances, the bands are multiply connected at the high-symmetry points Γ and X. The distortion from the B1 to the ideal B20 structure transforms the straight lines to zigzag chains with equal distances, lifts the degeneracy of the bands, and permits the opening of a gap. The distortion from the ideal to the real B20 structure splits the shell of seven equidistant nearest Pd neighbors around each Al at 2.63 Å into $1+3+3$ neighbors located at increasing distances of 2.58, 2.60, and 3.04 Å. The distortion corresponds to a dimerization of the . . .-Al-Pd-Al-Pd-. . . chains with alternating short (2.60 Å) and long (3.04 Å) distances. It leads to a stronger hybridization between Pd-d and Al-p states and enhances the covalent character of the Al-Pd bonds and the stability of the B20 over the B1 structure.[36] Figure 2 shows contour plots of differential electron densities of FeSi and AlPd. In the differential electron density a superposition of atomic charge densities is subtracted from the self-consistent charge density distribution. In Fig. 2 the differential electron density visualizes the covalency of the interatomic bonding in the dimerized Fe-Si and Al-Pd chains as shown by the formation of density maxima in the midpoint between the atoms. It is seen that in FeSi covalency is more pronounced than in AlPd.

In B20 the nearest-neighbor bonds form zigzag chains running parallel to the Cartesian axes (the twofold symmetry axes). A similar type of bonding has been observed in face-centered icosahedral quasicrystals such as Al-Pd-Re[36] where the individual Al-TM bonds are also oriented along the icosahedral threefold directions and dimerized zigzag chains of bonds run along the icosahedral twofold symmetry directions. Hence the experimentally reported semiconductivity of icosahedral Al-Pd-Re[37] has the same origin as that of FeSi in the B20 structure.[36]

IV. STRUCTURE AND STABILITY OF SURFACES IN B20-TYPE COMPOUNDS

In closely packed cubic crystals the low-index surfaces {100}, {110}, and {111} are found to exhibit the highest stability. Crystalline layers with these orientations are densely

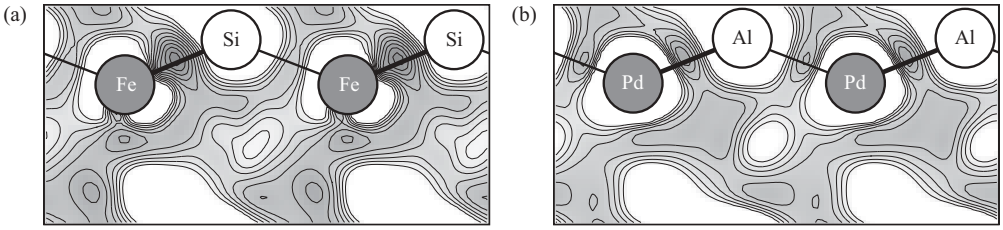

FIG. 2. Contour plot showing the differential electron density in (a) FeSi and (b) AlPd with the B20 structure. For alternating strong short and weak long bonds in the zigzag Fe-Si and Al-Pd chains are manifest as maxima in the differential electron density. See text.

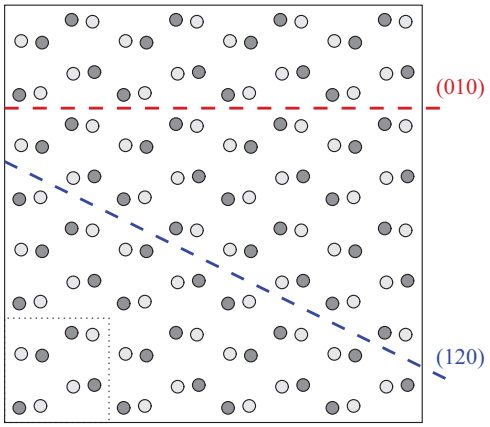

FIG. 3. (Color online) Side view of the layered structure of AlPd projected onto the (001) plane. The blue dashed line shows the position of the cleavage plane determining the pseudo-fivefold (120) surface, the red dashed line the cleavage plane for the formation of a (010) surface perpendicular to a twofold screw axis. The dotted square marks one unit cell.

populated and separated by relatively large distances. The situation is different for the B20 structure. Perpendicular to the ⟨110⟩ directions there are many sparsely occupied atomic planes at small distances such that formation of a surface with this orientation not likely. In the B20 compounds a role analogous to the {110} surface in the closely packed B2 structure is played by the {210} surface exhibiting a pseudo-fivefold symmetry. In the following we present our results for the twofold {100}, the pseudo-fivefold {210}, and the polar threefold {111} and $\{\bar{1}\bar{1}\bar{1}\}$ surfaces.

A. Twofold {100} surface

Perpendicular to the ⟨100⟩ directions in AlPd one finds a sequence of atomic planes with alternating distances of 0.97 Å and 1.49 Å; see Fig. 3. If the crystal is cleaved between the planes separated by the larger distance, the {100} surface is formed by a bilayer of two separated by 0.97 Å. Relaxation reduces this distance to 0.76 Å and increases the distance to the next bilayer; see Table II. All atomic planes are slightly puckered. The corrugation h of the surface defined as the difference between the positions of the highest and lowest surface atom is 0.83 Å, slightly larger than the relaxed

TABLE II. Interlayer distances d_{12}, d_{23}, and d_{34} and surface energies γ of the (100) and (210) surfaces of AlPd in the B20 structure. For comparison, data for surfaces of constituent elements are also presented. The first value gives the optimized distance between the near-surface layers; the number in parentheses are the corresponding bulk values. See Fig. 5.

Surface	d_{12} (Å)	d_{23} (Å)	d_{34} (Å)	γ (J/m^2)
AlPd(100)	0.76(0.97)	1.59(1.49)	0.90(0.97)	1.31
AlPd(210)	2.18(2.20)	2.19(2.20)		1.43
Al(100)	2.06(2.02)	2.04(2.02)		0.91
Al(111)	2.39(2.34)	2.35(2.34)		0.77
Pd(100)	1.95(1.98)	1.97(1.98)		1.51
Pd(111)	2.29(2.28)	2.27(2.28)		1.33

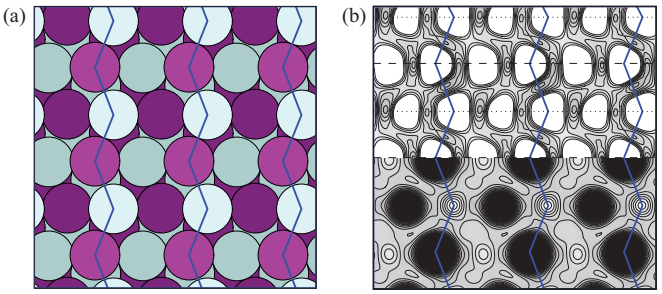

FIG. 4. (Color online) (a) Top view of the twofold (010) surface of AlPd. A surface area of 3×3 surface cells is shown. Positions of atoms are shown by circles: Al, light blue; Pd, magenta. The atoms below the top surface layer are darker. The corrugated surface is formed by zigzag chains of Al-Pd atoms separated by shallow valleys. (b) The total (bottom) and differential (top) valence electron density. The differential electron density shows that zigzag chains of bonds with enhanced covalency extend in both Cartesian directions parallel to the surface: [001] (full zigzag lines) and [100] (dashed and dotted lines).

distance of 0.76 Å between the two top planes. Figure 4(a) presents a top view on the (010) surface formed by zigzag chains of Al-Pd atoms separated by intervals permitting to see the zigzag chains in the layer 0.76 Å below. Figure 4(b) shows the total and differential valence electron density. The differential electron density demonstrates that chains of bonds with enhanced covalency propagate both along the [001] (full zigzag lines) and the [100] Cartesian directions (dashed and dotted lines). The Al-Pd chains perpendicular to the [010] direction are terminated by the surface. Perpendicular to the twofold surface there is thus one "dangling" bond per atom.

The surface cell is a square of 4.91 Å × 4.91 Å and contains two Al and two Pd atoms. The composition of the surface is thus the same as that of the bulk. One can construct a stoichiometric slab terminated on both by the same surface. We have calculated the surface energy using a symmetric slab containing 16 atomic planes. The outermost layers have been relaxed. The interlayer distances change appreciably, but we find no surface reconstruction (see Table II). The calculated surface energy of the {100} surface of AlPd is 1.31 J/m^2. For comparison, the surface energies of the most stable surfaces of constituent elemental metals Al and Pd are γ[Al(111)] = 0.77 J/m^2 and γ[Pd(111)] = 1.33 J/m^2.

B. Pseudo-fivefold surface {210}

Perpendicular to the [120] direction the B20 structure consists of a stacking of slightly puckered planes containing Al and Pd atoms in equal numbers, separated by a gap of 2.195 Å; see Fig. 3. The atomic arrangement in these planes has pseudo-fivefold (p5f) symmetry; the angle between the pseudo-fivefold direction and the [100] direction is β, $\sin\beta = \tau/\sqrt{\tau+2}$, $\beta = 58.28°$, where τ is the golden mean. This angle differs only slightly from the 60° between the [100] and [120] directions. After relaxation the distance d_{12} to the first Al-Pd subsurface layer is 2.18 Å, almost unchanged with respect to the bulk (see Fig. 5 and Table II). The p5f planes are quite strongly corrugated (see Fig. 5) with an amplitude of $h = 0.68$ Å in the bulk. Relaxation reduces the puckering of the top surface layer to 0.61 Å, but hardly affects the

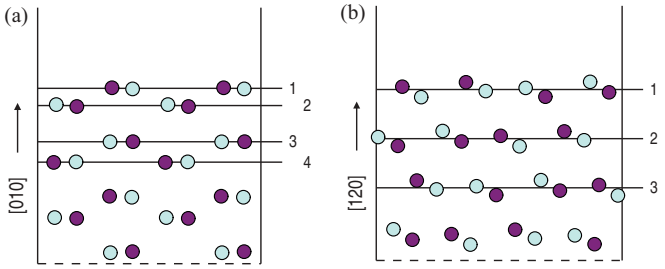

FIG. 5. (Color online) Side view of the optimized structures of the (010) (a) and (120) (b) surfaces of AlPd. The interplane distances between the top atomic planes marked 1 to 4 are given in Table II. The violet circles mark positions of Pd atoms, the light-blue circles Al atoms.

lateral distances between the atoms in the surface layer. The opposite pseudo-fivefold surfaces differ by chirality; otherwise the structural characteristics and the chemical composition are the same.

Figure 6 shows a top view of the p5f surface. The ordering of atoms in the surface layer can be described by a tiling consisting of golden thick rhombi and squashed hexagons (RH tiling), the vertices being occupied alternatingly by Al and Pd atoms. The acute angles in the rhombi and the hexagons are $2\pi/5$. If each hexagon is decomposed into one golden thick rhombus and two golden thin rhombi [see the dashed lines in Fig. 6(a)] one gets the Penrose tiling. In the Penrose tiling vertices linked by the short diagonal of a thin rhombus are left vacant. Alternatively, if each thick rhombus is split into two triangles and each hexagon is decomposed into two triangles and one rectangle (see the full red lines in Fig. 6), one gets a rectangle-triangle (RT) tiling with atoms at all vertices.

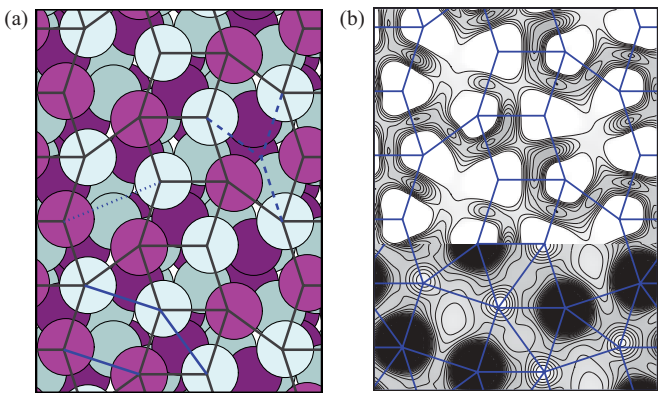

FIG. 6. (Color online) (a) Top view of the pseudo-fivefold (120) surface of AlPd. A surface area of 3 unit cells is shown. Positions of atoms are shown by circles: Al, light blue; Pd, magenta. The arrangement of the atoms in the surface layer can be described by different planar tilings: (i) a tiling consisting of thick golden rhombi and hexagons [RH tiling, full blue (dark) lines], or (ii) a rectangle-triangle (RT) tiling if all hexagons and rhombi are split as indicated by full blue (gray) lines. (iii) The hexagonal tile can also be divided into one thick and two thin rhombi (as shown by the dashed lines), producing a Penrose tiling. (iv) If the hexagons are split into two irregular quadrangles (as shown by the dotted line), the tiling can be described as arising from a distortion of the tiling describing the (110) surface of the B2 structure. (b) The total (bottom) and differential (top) valence electron density in the surface plane. The differential electron density demonstrates the partially covalent character of the Al-Pd bonds in the surface plane, directed along the edges of the RH tiling.

If the hexagons are split into two irregular quadrangles [see the dotted line in Fig. 6(a)] one creates a tiling that allows us to see the relation with the (110) surface of the B2 structure. If the positions of the atoms in the surface layer are shifted a little such that all quadrangular tiles become rectangular, the structure becomes identical to that of the (110) B2 surface. The (210) surface of the B20 structure thus plays a role analogous to the intensively studied (110) surface of B2-type Al-TM compounds.[38,39]

It is possible to assign a parity to each vertex in the RH tiling. If the Al atoms are placed on the "odd" vertices, the Pd atoms occupy vertices with "even" parity. Moreover, there are two kinds of Al sites and two kinds of Pd sites. Pd sites of the first kind have three Al neighbors; Pd sites of the second kind have four Al neighbors (see the number of RH edges with a common vertex). Each Pd site of the second kind is located in the center of an incomplete pentagon of Al atoms: Four Al atoms occupy the vertices of a regular pentagon; the fifth is replaced by an Al-Pd pair occupying one edge of a rectangular tile. This configuration resembles the pentagonal configurations of atoms on the catalytically active (100) surface of $Al_{13}Co_4$.[17]

In Fig. 6(b) the differential electron density demonstrates that on the p5f surface the covalent Al-Pd bonds are oriented essentially along the edges of the RT tiling. In the bulk each Pd atom is covalently bonded to six Al neighbors. On the p5f surface one half of Pd atoms has four Al neighbors; the other half has three Al neighbors only. From the remaining bonds one half is directed below and the other half above the surface. The same counting holds also for the Al atoms. On average, at the (210) there are thus 1.25 dangling bonds per atom.

C. Threefold surface {111}

Perpendicular to the [111] direction the period of the B20 structure is equal to the body diagonal of the cubic elementary cell, $d = a\sqrt{3}$. In each period there are nine atomic planes

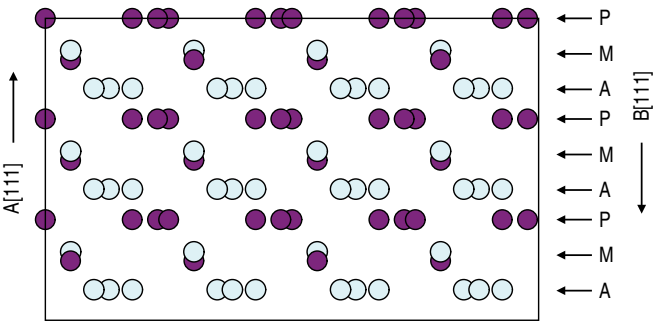

FIG. 7. (Color online) The layered structure of AlPd along the polar [111] direction. A view of two elementary cells along horizontal direction [10$\bar{1}$] are presented. This side view along [$\bar{1}$2$\bar{1}$] of enantiomorph A can be alternatively understood as a mirror image of enantiomorph B rotated by 180°. Positions of atoms are shown by circles: Al, light-blue; Pd, violet. In one period perpendicular to [111] there are nine atomic layers: three flat occupied by Pd only (P), three flat Al layers (A), and three layers with mixed Al-Pd occupancy (M).

(see Fig. 7): three flat planes occupied by Al only (A), three flat planes occupied by Pd atoms only (P), and three slightly puckered planes with mixed Al-Pd occupancy (M). The flat planes have three atoms per hexagonal surface cell; the mixed M planes with only two atoms per hexagonal cell are sparser.

As already noted (Sec. III) the B20 structure exists exists in two enantiomorphic forms labeled A or B. (Rosenthal *et al.*[25] investigated the surface properties of a GaPd sample of the B form.) Along the [111] direction the enantiomorphs have different chirality. In the following we shall distinguish, where this is necessary, the threefold directions by a prefix A or B. In energetic considerations the A[111] direction is equivalent to the B[$\bar{1}\bar{1}\bar{1}$] direction and vice versa. Figure 7 shows the stacking of different atomic layers along the [111] direction.

The $\{111\}$ surfaces have a polar character. The surfaces terminations oriented in the [111] direction are different from those looking in the opposite [$\bar{1}\bar{1}\bar{1}$] direction. Altogether, we recognize six possible surface terminations with different atomic planes in the surface and subsurface positions: three terminations with AP, MA, and PM bilayers perpendicular to the A[111] direction (normal vector of the surface plane) and three terminations with MP, PA, and AM bilayers perpendicular to the normal A[$\bar{1}\bar{1}\bar{1}$].

Alternatively, the puckered M layer can be considered as consisting of two very sparse planes with only one atom per hexagonal surface cell. We shall denote these subplanes by lowercase letters "a" for Al and "p" for Pd plane; i.e., M = a + p. This would require distinguishing four additional surface terminations—aA, pA, aP, and pP. Because the simulated cleavage process (to be described in more details below) did not result in a splitting of the M layer we shall consider it one puckered atomic plane. The bulk value of the puckering is 0.25 Å. However, in Sec. IV C3 we have also examined the possibility that atoms from one of the subplanes desorb when the M layer is exposed at the surface.

The atomic density in either the P, A, or M planes is not sufficient to form a stable surface. The $\{111\}$ surfaces consist of bilayers formed by two atomic planes. The AP and PA surfaces are formed by A and P planes in different stacking sequences. The valence electron distributions in both surfaces are characteristically different, as illustrated by Fig. 8. On the AP bilayer one observes in addition to the delocalized electron density of the Al atoms in the top layer also contributions from the localized electron density of the Pd atoms in the second layer. In contrast the valence electron density on the PA bilayer is dominated by the Pd contributions, with broad density minima above the Al triangles in the second layer. The differential electron density shown in the top parts of Fig. 8 demonstrates that in both surfaces each Pd is covalently bonded to three neighboring Al atoms. Of the remaining three Pd-Al bonds on average one half is oriented toward the deeper layers and the second half points out of the surface plane. At the threefold surfaces we have thus on average 1.5 "dangling" bonds per Pd (or Al) atom. Views of the atomic structure of all $\{111\}$ surface terminations are presented in Figs. 9–11.

Because of the substantially lower surface energy of face-centered cubic (fcc) Al(111) surface than of the fcc Pd(111) surface, it can be expected that Al-rich terminations have in general a lower surface energy than the Pd-rich terminations. Similarly, the formation of surfaces with a low corrugation should be preferred to the formation of highly corrugated surfaces. From these general arguments one would expect that the most stable (111) surface is terminated by an AM bilayer and the most stable ($\bar{1}\bar{1}\bar{1}$) surface by an AP bilayer.

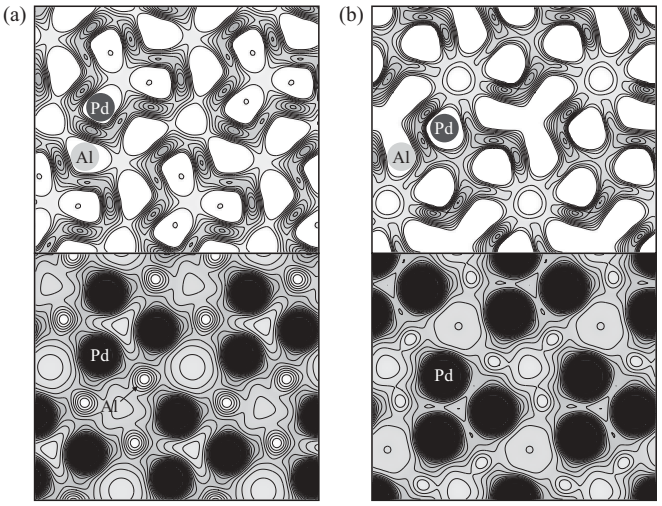

FIG. 8. Total and differential valence electron densities in the surface planes of (a) AP and (b) PA surfaces. The total valence electron density (bottom) shows that in the surface plane there are contributions from both Al and Pd atoms, but significantly smaller Al contributions for the PA surface. The differential electron densities (top) show the partially covalent character of the Al-Pd bonding in the surface plane: Each Pd atom is bonded to three neighboring Al atoms.

In general for a layered crystal structure one expects cleavage will lead to the formation of the surface with the lowest energy. However, because of the polar character of the $\{111\}$ surfaces of the B20 structure, different surfaces are exposed on both sides of the cleavage plane. Perpendicular to the [111] direction there are three possible cleavage planes

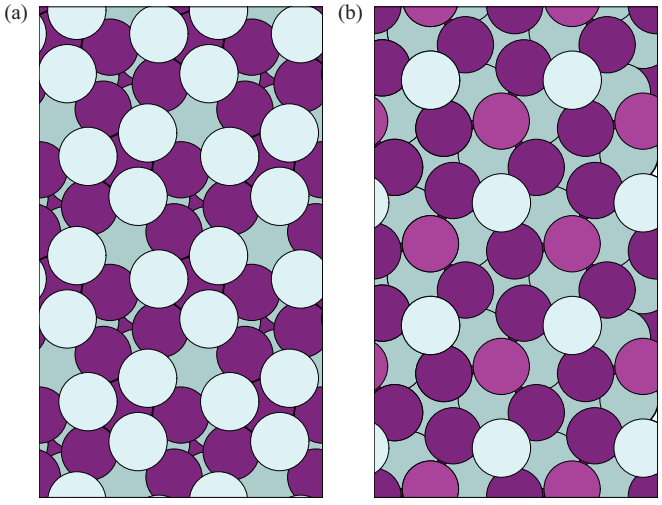

FIG. 9. (Color online) Top view of threefold surfaces of AlPd terminated by (a) AP and (b) MP bilayers. A surface area of 2×2 rectangular unit cells is shown. The violet circles mark the positions of Pd atoms; the light-blue circles are Al atoms. Atoms in the subsurface layers are darker. The diameters of the circles are 2.86 Å and 2.75 Å for Al and Pd atoms, respectively.

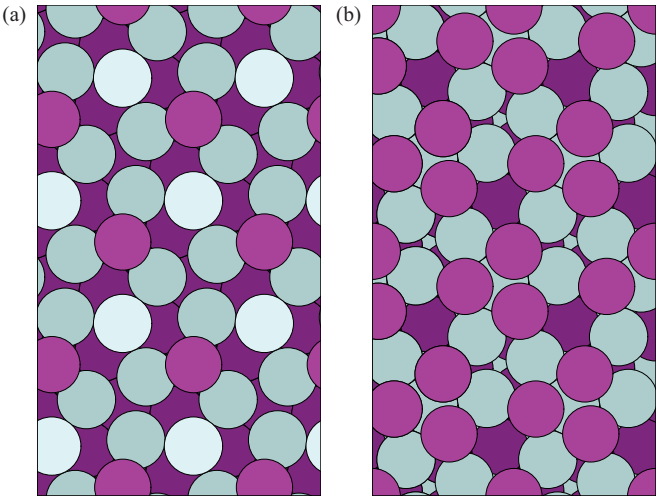

FIG. 10. (Color online) Top view of threefold surfaces of AlPd on both side of a possible cleavage plane: (a) MA termination, (b) PA termination. A surface area of 2×2 rectangular unit cells is shown. The violet circles mark the positions of Pd atoms; the light-blue circles are Al atoms. The atoms in the subsurface layers are darker.

leading to the formation of AP/MP, MA/PA, and PM/AM surface pairs.

Figures 9, 10, and 11 shows the atomic structure of the opposite surfaces for the three different cleavage planes. All surfaces are fully relaxed. The lateral positions of atoms at the relaxed surfaces do not differ too much from the positions at the unrelaxed bulk terminated surfaces. Changes of the lateral positions of atoms at the MA and MP surfaces are essentially negligible. Other surface terminations in the top atomic layer expose characteristic triplets of atoms. In the bulk structure the atoms in the triplets are second-nearest neighbors. The bulk distances between Al-Al and Pd-Pd pairs in the triplets are 3.04 Å and 3.02 Å, respectively. At the relaxed surfaces Pd-Pd distances shrink by 2.9% (PM) or 2.2% (PA). Al-Al distances increased at the AP surface by 3.4% but at the AM surface decreased by 3.3%. This is quite remarkable as our

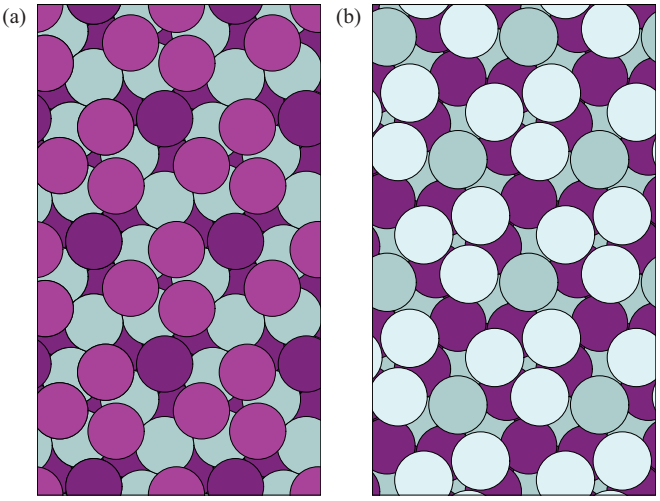

FIG. 11. (Color online) Top view of the threefold surfaces of AlPd on both sides of a possible cleavage plane: (a) PM, (b) AM surface. See Fig. 10.

preliminary results for GaPd indicate that the Ga-Ga distances at the relaxed threefold surfaces are substantially larger in comparison with their bulk distances.

1. Simulated cleavage experiment

To determine the preferred cleavage plane we have simulated the cleavage process of the B20 crystal by applying an increasing tensile deformation of the computational cell along the [111] direction. The cell was extended first by $d/2$, the forces acting in the atoms were relaxed, and then the cell was extended again by $d/2$. As the sparse M planes tend to become laterally unstable during the tensile deformation we fixed the lateral positions of the atoms. For more computational details the reader is referred to our previous study of the formation of the (100)-$Al_{13}Co_4$ surface[15] where we employed the same simulation of the cleavage process.

The simulation showed that the AlPd crystal cleaves along the MA/PA plane between the highly corrugated Al-rich MA and the low-corrugated Pd-rich PA surfaces. The low-corrugated Al-rich AP surface which is expected to have the lowest surface energy (as also confirmed by the calculations described below) was not created during the cleavage process. Exposure of the AP surface would require cleavage at the AP/MP plane and the simultaneous formation of the opposite highly corrugated and Pd-rich MP surface; see Fig. 9. Calculations of the surface energies described in Sec. IV C3 confirm that the average surface energy of the MA and PA surfaces is lower than that of the AP and MP surfaces.

The cleavage experiment has demonstrated that to achieve a deeper understanding of the formation of the polar threefold surfaces of the B20 structure it is not enough to determine the surface with the lowest surface energy but it is important to know also surface energies of other possible surface terminations. Cleavage and crystal growth can lead to the formation of different surfaces. At elevated temperatures the surface of a crystal can also be modified by a selective desorption.

2. Layered structure of threefold surfaces

Figure 12 shows side views of the threefold surfaces on both sides on one of the three possible cleavage planes. The stoichiometries of the surface bilayer and the interplanar distances after relaxation and in the bulk are summarized in Table III. The distances d_{12} between the surface and subsurface planes are always contracted relative to the bulk, except for the MA surface where the corrugation of the mixed M layer is with 0.37 Å higher than the bulk value of 0.25 Å. If the M layer is in a subsurface position its corrugation is also substantially increased; the maximal value of $d_{34} = 0.46$ Å is observed for the AP surface. On the other hand the distance between the denser A and P planes (0.86 Å in the bulk) is reduced not only at the surface but also in subsurface positions.

3. Surface energies

The surface energy γ can be directly derived from slab calculations, provided that the stoichiometry of the slab used to represent the surface is the same in the bulk and if both surfaces—top and bottom—are the same. As the (111) surfaces of the B20 crystal have polar character one can construct

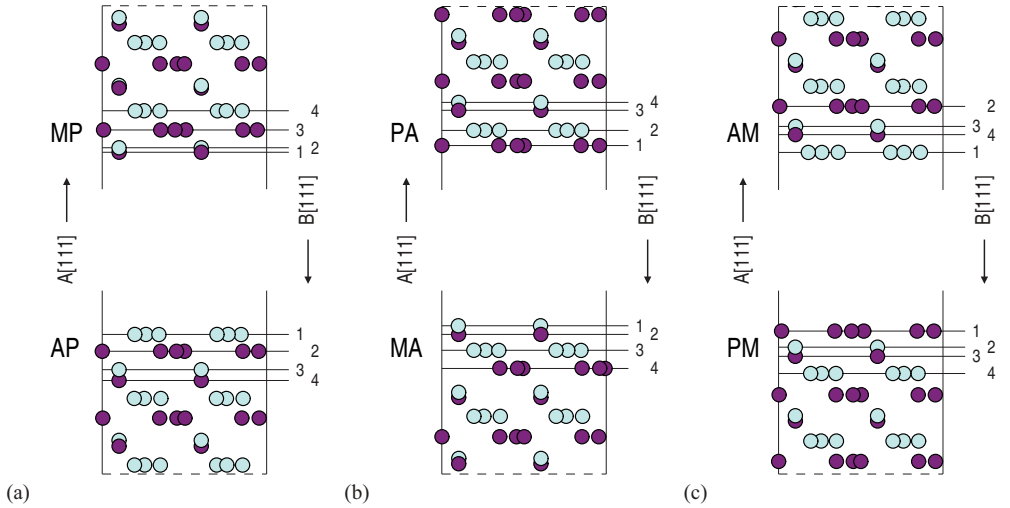

FIG. 12. (Color online) Side views of the threefold surfaces on both sides of a (111) cleavage plane of AlPd: (a) AP and MP, (b) MA and PA, (c) PM and AM. The interplanar distances between the four near-surface layers marked 1 to 4 are given in Table III. The violet circles mark positions of Pd atoms; the light-blue circles are Al atoms.

only stoichiometric slabs with different surfaces on both sides terminations. If one surface is formed by one of the possible (111) terminations the other surface must be formed by one of the $(\bar{1}\bar{1}\bar{1})$ terminations. Hence one can directly calculate only an average surface energy of both surfaces of the slab. For instance, if a stoichiometric slab is terminated on both sides by a mixed Al-Pd layer M, the subsurface layer is occupied by Pd atoms on one and by Al atoms on the other side. Hence one can calculate only the average energy of the MP and MA surfaces.

Altogether there are nine possibilities to construct a slab: each of the three A(111) terminations (AP, MA, PM) can be combined with any of the A$(\bar{1}\bar{1}\bar{1})$ the terminations (MP, PA, AM). Out of these nine combinations five define a stoichiometric slab. Three of them—AP + MP, MA + PA, and PM + AM—correspond to the three possible cleavage planes. The remaining two stoichiometric slabs AP + PA and MA + MP are obtained if the mixed M layer or a pair of A and P planes are deleted from the bulk structure. The calculated average surface energies $\bar{\gamma}$ for all five stoichiometric combinations are listed in Table IV.

The highest average surface energy of $\bar{\gamma}(\mathrm{PM}+\mathrm{AM}) = 1.96\ \mathrm{J/m^2}$ is calculated for the slab terminated by PM and AM surfaces. The lowest average surface energy of $\bar{\gamma}(\mathrm{PA}+\mathrm{AP}) = 1.56\ \mathrm{J/m^2}$ was found for a slab with PA and AP surfaces which cannot be generated by a periodically repeated cleavage terminations. Cleavage leads to the formation of MA and PA surfaces with an average surface energy of $\bar{\gamma}(\mathrm{MA}+\mathrm{PA}) = 1.60\ \mathrm{J/m^2}$; consistent with the result of the simulated cleavage experiment this is the lowest average surface energy for any possibility to cleave the crystal perpendicular to the [111] direction. As already noted formation of the AP surface by cleavage is possible only in combination with the simultaneous formation of an MP surface, leading to a higher average surface energy of $\bar{\gamma}(\mathrm{AP}+\mathrm{MP}) = 1.69\ \mathrm{J/m^2}$.

Using the grand-canonical formalism[40–42] the surface energies of nonstoichiometric slabs can be be expressed as a function of the chemical potentials of both components

$$\gamma = \left(E^s - N^s_{\mathrm{Al}}\mu_{\mathrm{Al}} - N^s_{\mathrm{Pd}}\mu_{\mathrm{Pd}}\right)/A, \qquad (1)$$

where E^s is total energy of the slab from the DFT calculations, N^s_{Al} and N^s_{Pd} are the numbers of Al and Pd atoms in the slab, μ_{Al} and μ_{Pd} are the chemical potentials of both elements in the reactive atmosphere above the surface, and A is the surface area of both sides of the slab. The chemical potentials μ_{Al} and μ_{Pd} can vary only within certain intervals. Thermal equilibrium

TABLE III. Stoichiometries, interlayer distances, and surface energies of the threefold surfaces of AlPd. N_{Al} and N_{Pd} are number of atoms in the surface bilayer per hexagonal surface cell; d_{12}, d_{23}, and d_{34} are interplanar distances between the four topmost atomic planes for the relaxed surfaces and their bulk values (in parentheses). The last column lists the estimated values $\tilde{\gamma}$ of the surface energies; see text.

Surface	N_{Al}	N_{Pd}	d_{12} (Å)	d_{23} (Å)	d_{34} (Å)	$\tilde{\gamma}$ (J/m^2)
A(111), B$(\bar{1}\bar{1}\bar{1})$						
AP	3	3	0.71(0.86)	0.78(0.91)	0.46(0.25)	1.37
MA	4	1	0.37(0.25)	0.67(0.81)	0.77(0.86)	1.46
PM	1	4	0.68(0.91)	0.39(0.25)	0.73(0.81)	2.28
A$(\bar{1}\bar{1}\bar{1})$, B(111)						
MP	1	4	0.19(0.25)	0.75(0.91)	0.80(0.86)	2.01
PA	3	3	0.65(0.86)	0.84(0.81)	0.33(0.25)	1.75
AM	4	1	0.75(0.81)	0.35(0.25)	0.85(0.91)	1.65

TABLE IV. Average surface energies $\bar{\gamma}$ for the surfaces on both sides of stoichiometric slabs. See text.

Surfaces		Average surface energy
A(111), B($\bar{1}\bar{1}\bar{1}$)	A($\bar{1}\bar{1}\bar{1}$), B(111)	$\bar{\gamma}$ (J/m^2)
AP	MP	1.68
MA	PA	1.60
PM	AM	1.96
AP	PA	1.56
MA	MP	1.73

with the bulk AlPd crystal is expressed by the condition

$$\mu_{\mathrm{Al}} + \mu_{\mathrm{Pd}} = g_{\mathrm{AlPd}}, \tag{2}$$

where $g_{\mathrm{AlPd}} = -10.75$ eV is the cohesive energy of AlPd per formula unit. If the chemical potential μ_{Al} is too high compact Al islands can be formed on the surface; therefore $\mu_{\mathrm{Al}} \leqslant g_{\mathrm{Al}}$, and similarly $\mu_{\mathrm{Pd}} \leqslant g_{\mathrm{Pd}}$, where $g_{\mathrm{Al}} = -3.70$ eV and $g_{\mathrm{Pd}} = -5.21$ eV are the cohesive energies of Al and Pd in their stable fcc phases. These conditions and Eq. (2) determine the possible values of the chemical potentials:

$$-5.53 \text{ eV} \leqslant \mu_{\mathrm{Al}} \leqslant -3.70 \text{ eV}, \tag{3}$$

$$-7.05 \text{ eV} \leqslant \mu_{\mathrm{Pd}} \leqslant -5.21 \text{ eV}. \tag{4}$$

Unfortunately, extension of the calculations of surface energies to nonstoichiometric slabs does not help to separate the values for individual surfaces. The problem is that the calculated average surface energies are correlated. Since the slab is always terminated by surfaces belonging to two opposite threefold directions the surface energies of the (111) surfaces always depend on the surface energy of the ($\bar{1}\bar{1}\bar{1}$) surfaces and vice versa. There are only three independent values, e.g., those corresponding to the three possible cleavage planes. It is very instructive to consider this correlation between the surface energies. Figure 13(a) presents the variation of the surface energies for the AP, MP, MA, and PA surfaces as a function of the assumed value of the energy of the AP surface. Figure 13(b) shows the dependence of the surface energies for PM/AM cleavage as a function of the energy of the AM surface.

The surface energy depends significantly on the chemical composition of the surface. From Figs. 9(b) and 10(a) it is obvious that on the MA and MP surfaces the atoms in the sparse M layer occupy sites in the broad threefold hollows between the Al triplets and Pd triplets in the subsurface A and P layer, respectively. The triplets from the subsurface layer remain exposed at the surface. Hence the MA surface contains eight Al atoms and two Pd atoms per a rectangular surface cell (corresponding to two primitive hexagonal surface cells) and vice versa for the MP surface. The MA (MP) surface is thus Al (Pd) rich. The MA and MP surfaces are essentially isostructural and differ only by inversion of the chemical types. Using this fact one can estimate the energies of individual surfaces. For the (111) surfaces of the face-centered cubic metals, the calculated surface energies are $\gamma[\mathrm{Al}(111)] = 0.77\,\mathrm{J/m^2}$, which is much lower than $\gamma[\mathrm{Pd}(111)] = 1.33\,\mathrm{J/m^2}$. Assuming that the surface energies of the Al-, respectively Pd-rich MA and MP surface terminations, are in a proportion corresponding to the concentration-weighted surface energies of the pure metals,

$$\frac{\gamma(\mathrm{MA})}{\gamma(\mathrm{MP})} \approx \frac{0.8\gamma[\mathrm{Al}(111)] + 0.2\gamma[\mathrm{Pd}(111)]}{0.2\gamma[\mathrm{Al}(111)] + 0.8\gamma[\mathrm{Pd}(111)]}, \tag{5}$$

and using their average value of $\bar{\gamma}(\mathrm{MA}+\mathrm{MP})$, see Table III, one can estimate the individual surface energies for four of the six (111) or ($\bar{1}\bar{1}\bar{1}$) surfaces. The concentration factors 0.8 and 0.2 correspond to the concentration of Al and Pd atoms in the bilayers of the MA and MP surface terminations. The same approach can be applied also to the PM and AM surfaces which are also essentially isostructural and differ by only by inversion of the chemical types.

Figure 13 demonstrates that even if the estimated values of the surface energies should not be too accurate, the order of the surface energies remains the same. To distinguish the estimated surface energies from those calculated directly we denote them as $\tilde{\gamma}$. The accuracy of the estimated surface energies are discussed in Sec. VI. As expected the Al-rich surfaces AP, MA, and AM have lower surface energies than the Pd-rich terminations PA, MP, and PM.

Using the grand-canonical formalism [Eqs. (1) and (2)] one can calculate the surface energies of nonstoichiometric slabs for the limiting values of the chemical potentials. For instance, for a slab with PM and MP surfaces we calculated average surface energies in the range $1.25\,\mathrm{J/m^2} \leqslant \bar{\gamma}(\mathrm{PM}+\mathrm{MP}) \leqslant 2.31\,\mathrm{J/m^2}$. On the other hand, using this formalism and the estimated values of $\tilde{\gamma}$(PM) and $\tilde{\gamma}$(MP) (see Table III) one can derive the corresponding values of the chemical potentials: $\tilde{\mu}_{\mathrm{Al}} = -3.98$ eV and $\tilde{\mu}_{\mathrm{Pd}} = -6.76$ eV. Both values are within the limits imposed by the equilibrium conditions [see Eqs. (3) and (4)] for the chemical potentials. Since the individual surface energies are mutually dependent the calculated values of the chemical potentials are the same (within an accuracy $\approx$1% of the calculated values of the surface energies), regardless of the choice of the surface terminations for the nonstoichiometric slab. The approximation Eq. (5) is thus essentially equivalent to an estimation of the values of the chemical potentials.

From Fig. 13 and Table III one concludes that the most stable A(111) surface termination is the AP bilayer with an estimated surface energy of $\tilde{\gamma}(\mathrm{AP}) = 1.37\,\mathrm{J/m^2}$. The lowest surface energy for the opposite direction is found for the AM termination with $\tilde{\gamma}(\mathrm{AM}) = 1.65\,\mathrm{J/m^2}$.

4. *Change of surface composition by partial desorption*

So far we have not considered a possible desorption of atoms from the surface. If the surface is prepared at high temperatures part of the surface atoms can desorb. One can assume that atoms from the sparse M plane of the highly corrugated MA and MP surfaces are most likely to desorb. While the MP surface with the highest surface energy of $\tilde{\gamma}(\mathrm{MP}) = 2.01\ \mathrm{J/m^2}$ out of all A($\bar{1}\bar{1}\bar{1}$) terminations will probably not be exposed at the surface, the case of the MA surface is worth of closer inspection. The surface energy of $\tilde{\gamma}(\mathrm{MA}) = 1.46\ \mathrm{J/m^2}$ is only slightly higher than the lowest value of $\tilde{\gamma}(\mathrm{AP}) = 1.37\ \mathrm{J/m^2}$ found for the A(111) surfaces. It is therefore possible that after desorption of some atoms

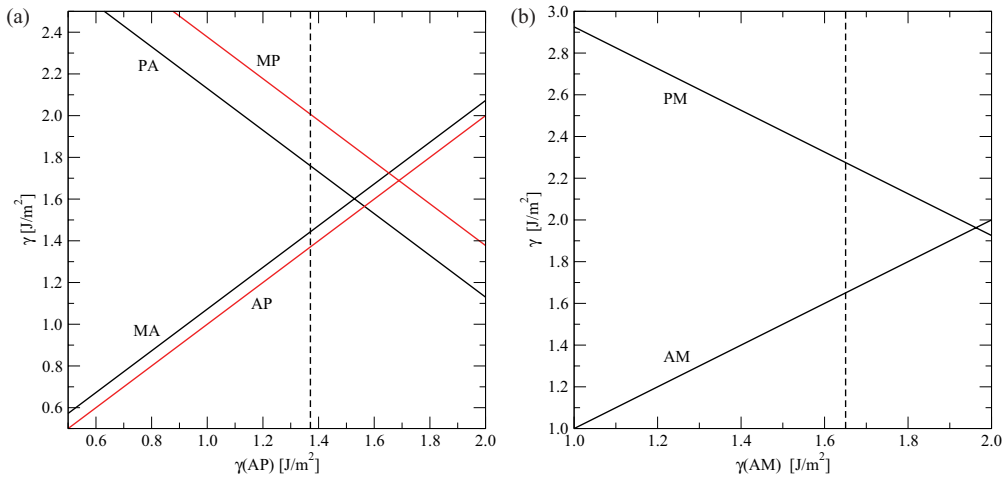

FIG. 13. (Color online) Mutual dependencies of the surface energies for the threefold surfaces of AlPd: (a) Variation of the surface energies γ for the MP, MA, and PA surfaces with the assumed value of γ(AP); (b) variation of the surface energy of the PM surface with the assumed value of γ(AM). The values of the surface energies estimated according to Eq. (5), $\tilde{\gamma}$, are given by the intersections with the dashed line; see text.

the surface energy will be reduced such that the modified MA surface becomes more stable than the AP termination.

The corrugated M layer consists of two subplanes; one has 1 Al atom and the other has 1 Pd atom per surface cell (M = a + p; see the beginning of Sec. IV C). To test whether Al or Pd desorption leads to a stronger reduction of the surface energy, we prepared two surface models denoted pA (desorption of Al) and aA (desorption of Pd). For both models the (111) surface is PA terminated. Both slabs are nonstoichiometric. From Eq. (1), the estimated values of the chemical potentials, and the energy of the PA surface (see Table III), one derives directly the surface energies. For the pA surface we obtained $\tilde{\gamma}(\mathrm{pA}) = 1.49$ J/m^2 and aA surface $\tilde{\gamma}(\mathrm{aA}) = 1.32$ J/m^2. Hence desorption of Al leads to an increased surface energy, while desorption of Pd reduces the surface energy such that it is even slightly lower than the lowest value of $\tilde{\gamma}(\mathrm{AP}) = 1.37$ J/m^2 for the bulk-terminated A(111) surfaces. The surface energy of the pure Al termination aA is thus comparable to that of the AP surface. In other words, the most stable A(111) surface can be understood as an AP surface where all (or a part of) the threefold hollows above Pd triples in the subsurface plane [see Fig. 9(a)] are occupied by adsorbed Al atoms.

5. *Atomically resolved STM images*

So far no experimental atomically resolved STM images of AlPd have been published. Nevertheless, it can be interesting to present the calculated STM images at least for the most stable threefold surfaces and compare them with available[43] experimental GaPd images. As the surfaces for recording of the STM images are usually prepared in ultrahigh vacuum at high temperatures the most likely observed A(111) surface will be the aA termination formed from MA after desorption of Pd atoms. However, as the estimated surface energy of aA is lower than that of AP by 0.05 J/m^2 only the latter surface termination can be exposed as well, particularly at lower temperatures. Figure 14 presents calculated STM images of both A(111) terminations with the competing surface energies. For the opposite direction A[$\bar{1}\bar{1}\bar{1}$] the lowest surface energy of was found for the AM surface termination. Figure 15 presents a calculated STM image of the A($\bar{1}\bar{1}\bar{1}$) AM surface termination. The images were calculated for fully relaxed surface structures and $U_B = -1.0$ eV.

The simulated images of aA and AM qualitatively agree well with those presented by Prinz *et al.*[43] for the threefold GaPd surfaces. However, our preliminary STM images calculated for the GaPd surfaces show that there are some significant quantitative differences between AlPd and GaPd threefold surfaces. While the lateral positions of Al atoms in the triplets at the fully relaxed AM termination, see Fig. 11, remain essentially at their bulk positions, in the case of the corresponding GaPd surface the distances between the Ga atoms in the triplets substantially (by 13%) increase. The puckering of the top A plane at the AM termination is substantially lower than that observed at the GaPd counterpart. The observed differences can be explained by the larger size of the Ga atoms.

V. EQUILIBRIUM SURFACE AREAS

Heterogenous catalysts are usually prepared in the form of small crystallites dispersed on an oxidic support. The equilibrium shape of the crystallites is determined by minimizing

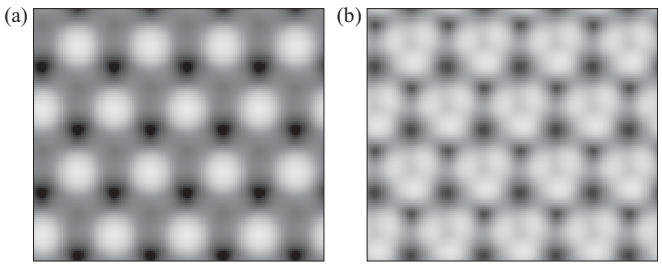

FIG. 14. Simulated STM images of the A(111) aA (a) and AP (b) surface terminations.

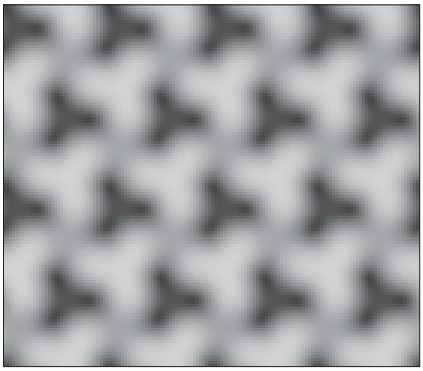

FIG. 15. Simulated STM images of the A($\bar{1}\bar{1}\bar{1}$) AM surface termination.

of the total surface energy at fixed volume of the crystallite. According to Wulff[44] the total surface energy is a minimum if the distance d_i of each facet from the center of the crystallite is proportional to the surface energy γ_i of the corresponding facet[45]

$$\frac{\gamma_i}{d_i} = \text{const.} \tag{6}$$

This is the basis for the Wulff construction of the shape of crystallites. The shape of very small crystallites might deviate from the prediction, as the contributions from the edges where the facets intersect are neglected, but experimental results indicate that crystallites with diameters of tens of nanometers are generally already consistent with this principle.[45]

Under the assumption that only twofold {100}, pseudo-fivefold {210}, and threefold {111} facets appear on the surface of AlPd crystallites and using their surface energies we have calculated the relative surface areas occupied by these facets. The results were obtained by numerical integrations and they are collected in Table V. A view of the crystallite is shown in Fig. 16.

The anisotropy of the surface energy along the threefold directions results in a substantial difference of the surface areas occupied by threefold facets with opposite orientations. The largest fraction is occupied by the {100} facets with the lowest surface energy, followed by the {210} facets and the A(111) facet with AP termination. We note that the calculations of the relative surface areas are for a freestanding crystallite. The surface energies and their anisotropy can change significantly in a gaseous or liquid environment.

VI. DISCUSSION AND CONCLUSIONS

In this work we have studied in detail low-index surfaces of the AlPd compound crystallizing in the B20 structure

TABLE V. Calculated surface energies and relative surface areas of the corresponding facets for AlPd crystallite (enantiomorph A).

Face	Multiplicity	γ (J/m^2)	Relative area
100	6	1.31	42%
210	12	1.43	35%
111	4	1.37	19%
$\bar{1}\bar{1}\bar{1}$	4	1.65	4%

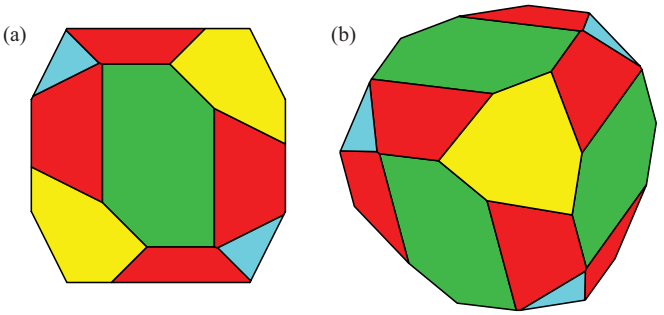

FIG. 16. (Color online) Equilibrium shape of a AlPd crystallite: (a) front view, (b) side view. Facets: {100}, green; {210}, red; A{111}, yellow; A{$\bar{1}\bar{1}\bar{1}$}, blue.

using *ab initio* density functional methods. We have presented structural details and surface energies of the twofold {100}, the threefold {111}, and the pseudo-fivefold {210} surfaces (which plays for the B20 structures a role similar to that of the {110} surfaces of the B2 structure). While all atomic layers perpendicular to the ⟨100⟩ and ⟨210⟩ directions are the same and therefore the question of the choice of the cleavage plane does not arise, for the threefold {111} surfaces the situation is much more complicated. The {111} surfaces have polar character. The surfaces oriented in the (111) direction differ from those oriented in the ($\bar{1}\bar{1}\bar{1}$) direction. Perpendicular to each of the opposite threefold directions there are several possible surface terminations.

The atomic structure of all investigated surfaces was optimized by relaxation of the interatomic forces. We have observed significant changes of interlayer distances close to the surface, but no surface reconstruction was found. As the lateral size of our computational cells was limited, long-period reconstructions cannot be excluded.

Chemical bonding in B20 compounds has at least partial covalent character. In AlPd dimerized zigzag Al-Pd chains extend parallel to the three twofold symmetry axes. The network of covalent bonds determines also the structure of the surfaces and permits an interpretation of the calculated surface energies in terms of "dangling" bonds.

The surface energies determine the relative stability of surfaces of different orientation and different positions of the cleavage plane. The chemical composition of the surface and the corrugation of the surface layer are the two most important factors influencing the surface energy. As the surface energy of fcc Al(111) is much lower than that of the fcc Pd(111) surface, it is expected that Al-rich surfaces of the AlPd compound have in general lower surface energy than Pd-rich terminations. Similarly, formation of surfaces with a low corrugation should be preferred to formation of highly corrugated surfaces. From these general arguments one would expect that the most stable surfaces are Al rich and show only a low corrugation.

For AlPd the lowest surface energy of 1.31 J/m^2 was calculated for the twofold {100} surface. The surface energy of the pseudo-fivefold {210} surface of 1.43 J/m^2 is somewhat higher. Both {100} and {210} surfaces have the same stoichiometry as the bulk crystal. It is interesting that although the twofold surface shows a higher corrugation than the pseudo-fivefold surface it has a lower surface energy. The reason is that the network of covalent Al-Pd bonds is less

disturbed by the formation of a {100} surface. In covalently bonded crystals surfaces with a higher number of dangling bonds per atom generally exhibit higher surface energies. While on the {100} surface there is one dangling bond per Pd atom, on the {210} surface we found on average 1.25 dangling bonds per Pd atom.

The polar character of the {111} surfaces complicates the calculation of the surface energies. All possible slab models have different surfaces on their (111) and $(\bar{1}\bar{1}\bar{1})$ side. Therefore all calculations yield only average surface energies $\tilde{\gamma}$ for the different surfaces on the opposite side of the slab. Using the assumption that the relation of the energies of surfaces with different composition is the same as that of the composition-weighted average of the surface energies of both constituent metals [see Eq. (5)] we were able to obtain estimated values $\tilde{\gamma}$ of the energies of individual surfaces.

The accuracy of these estimates is not easy to evaluate. However, certain assessment can be obtained considering the value of the surface energy of the {100} surface. The average of the (100) surface energies of Al (0.91 J/m^2) and Pd (1.51 J/m^2) is 1.21 J/m^2, i.e., by 8% smaller than the value of 1.31 J/m^2 calculated for the stoichiometric (100) surface of AlPd; see Table II. A comparison of the surface energies of the twofold {100} and the pseudo-fivefold {210} surfaces is also instructive. Both surfaces have the same chemical composition. Although the surfaces substantially differ in the structure and their interatomic bonding, their surface energies differ by 9% only. Since the structure and bonding of the MA and MP terminations are essentially the same one can assume that the deviations of γ(MA) and γ(MP) from their estimated values given by the approximation Eq. (5) will be smaller than 10%.

The lowest surface energy for the threefold A(111) surfaces was found for a surface with a bilayer formed by flat Al and Pd layers (the AP termination). Its estimated value is $\tilde{\gamma}$(AP) = 1.37 J/m^2. As the surface energy $\tilde{\gamma}$(MA) = 1.46 J/m^2 is only slightly higher surface terraces with the MA termination could coexist with the AP terraces. At high temperatures one can expect desorption of Pd atoms from the top M plane forming thus the Al-rich aA termination with the surface energy of $\tilde{\gamma}$(aA) = 1.32 J/m^2. Figure 14 presents simulated STM images of two A(111) terminations aA and AP with the competing surface energies. On the other A$(\bar{1}\bar{1}\bar{1})$ side, the lowest surface energy of $\tilde{\gamma}$(AM) = 1.65 J/m^2 was found for the termination AM. Here one can also speculate that the surface termination PA with a little higher surface energy of $\tilde{\gamma}$(PA) = 1.75 J/m^2 can coexist forming terraces with a relatively small surface area. The latter high values of the surface energies show that the polar threefold surfaces are strongly anisotropic.

The equilibrium shape of a crystallite has been determined from the Wulff construction. From Table V on can see that the surface of AlPd crystallites is dominated by twofold and pseudo-fivefold facets. The large surface area occupied by the (210) facets confirms our earlier work on the properties of AlPd as a catalyst for the semihydrogenation of acetylene to ethylene.[23]

To determine the preferable cleavage plane perpendicular to the (111) direction we have performed a simulated cleavage experiment. Quite surprisingly the preferred cleavage plane was found between the highly corrugated Al-rich MA and the low-corrugated Pd-rich PA terminations. The low-corrugated Al-rich AP surface with the lowest surface energy is not formed by the cleavage process. The explanation is obvious from Figs. 9 and 13(a). Cleavage at the AP/MP plane and formation of the AP surface is prevented by simultaneous formation on the opposite side of the cleavage plane of the highly corrugated and Pd-rich MP surface with a very high surface energy. We note that the situation is similar to that in $Al_{13}Co_4$, where the cleavage process results in the formation of a highly corrugated surface with the tops of the pentagonal bipyramidal cluster protruding form the surface while the formation of a flatter Al-rich surface is hindered the formation of a Co-rich surface with a high surface energy on the other side of the cleavage plane.[15]

While crystal growth will result in the formation of the surfaces permitting to minimize the total surface energy of a crystal, cleavage of a grown crystal can hence result in the formation of the Pd-rich PA surface despite its rather high surface energy. The morphology of the PA surface is particularly interesting. It consists of islands in the form of Pd triangles separated by shallow troughs. Our preliminary studies of its adsorption properties revealed that the Pd triplets strongly bind H atoms in their centers.

Our observations are in agreement with previous experience with surfaces of other Al-TM intermetallic compounds.[5–8,15] We have learned that formation of the surface of a complex crystal can depend significantly on the method of preparation. If the surface is prepared by crystal growth or in UHV by high-temperature annealing and ion-beam sputtering then the formation of Al-rich surfaces with the lowest surface energy is most likely. However, if the surface is created at low temperatures by a cleavage process then formation of a surface with the lowest surface energy can be hindered because it requires the simultaneous formation of a surface with much higher surface energy on the other side of the cleavage plane.

Very recently an experimental investigation of the structure of the threefold surface of B20-type GaPd using XPS, UPS, LEED, STM, and TPD of CO molecules has been published.[25] The experiments have been performed on a single crystal of the "B" enantiomorph grown by the Czochralski method. The orientation of the $(\bar{1}\bar{1}\bar{1})$ surface prepared by cutting and polishing was verified by x-ray diffraction. LEED and STM show that the surface has 1×1 periodicity; neither reconstruction nor segregation has been observed over a wide temperature range. Different surface terminations are observed for different annealing temperatures. A higher saturation coverage by CO has been observed on surfaces prepared at a lower temperature of 670 K. This has been attributed to termination of the surface by an outer layer containing three Ga or Pd atoms per surface cell. The desorption temperature from this surface is exceptionally low, with a dominant desorption peak at about 120 K. This could be assigned either to desorption of CO bound to Ga atoms, or from Pd atoms whose binding capacity is very strongly reduced by the covalent binding to Ga. Surfaces prepared at a higher temperature of 870 K show a strongly reduced saturation coverage of only one CO molecule per surface cell. The surface observed for the preparation at lower temperature could be interpreted in the light of our results as the AP or aA terminations with the lowest surface

energies of the three possible A(111) surfaces. However, this will require confirmation by adsorption studies. Although the GaPd compound is isostructural and isoelectronic to AlPd some preliminary results for this compound indicate that there are some significant differences. While for AlPd the lowest surface energy is found for the (100) surface, for GaPd the Ga-rich A(111) surface has the lowest energy. This could be related to the fact that a (111) surface of a hypothetical fcc Ga crystal has a surface energy that is even lower than that of the Al(111) surface. These investigations will be continued.

In summary, we have presented the results of detailed investigations of the low-index surfaces of B20-type AlPd. The lowest surface energies are predicted for the twofold (100) and the threefold Al-rich A(111) surfaces, with an only slightly higher value for the pseudo-fivefold (210) surface. The surface energies for the polar threefold surfaces are strongly anisotropic. In equilibrium nearly 80% of the surface of a AlPd crystal consists of (100) and (210) facets in nearly equal proportion; the reaction centers of AlPd catalysts for semihydrogenation of alkynes are found on the (210) surface.[23,24]

ACKNOWLEDGMENTS

This work has been supported by the Austrian Ministry for Science through the Center for Computational Materials Science. M.K. acknowledges also support from the Grant Agency for Science of Slovakia (No. 2/0111/11), from CEX FUN-MAT, and from the Slovak Research and Development Agency (Grants No. APVV-0647-10, No. APVV-0492-11, and No. APVV-0076-11). We thank Roland Widmer for valuable discussions.

[1] R. D. Diehl and R. McGrath, Surf. Sci. Rep. **23**, 43 (1996).
[2] R. McGrath, J. Ledieu, E. J. Cox, S. Haq, R. D. Diehl, C. J. Jenks, I. Fisher, A. R. Ross, and T. A. Lograsso, J. Alloys Compd. **324**, 432 (2002).
[3] O. Ourdjini, R. Pawlak, M. Abel, S. Clair, L. Chen, N. Bergeon, M. Sassi, V. Oison, J.-M. Debierre, R. Coratger, and L. Porte, Phys. Rev. B **84**, 125421 (2011).
[4] K. Kovnir, M. Armbrüster, D. Teschner, T. V. Venkov, F. C. Jentoft, A. Knop-Gericke, Y. Grin, and R. Schlögl, Sci. Technol. Adv. Mater. **8**, 420 (2007).
[5] R. Addou, E. Gaudry, Th. Deniozou, M. Heggen, M. Feuerbacher, P. Gille, Yu. Grin, R. Widmer, O. Gröning, V. Fournée, J.-M. Dubois, and J. Ledieu, Phys. Rev. B **80**, 014203 (2009).
[6] Th. Deniozou, R. Addou, A. K. Shukla, M. Heggen, M. Feuerbacher, M. Krajčí, J. Hafner, R. Widmer, O. Gröning, V. Fournée, J.-M. Dubois, and J. Ledieu, Phys. Rev. B **81**, 125418 (2010).
[7] E. Gaudry, A. K. Shukla, T. Duguet, J. Ledieu, M.-C. de Weerd, J.-M. Dubois, and V. Fournée, Phys. Rev. B **82**, 085411 (2010).
[8] Heekeun Shin, K. Pussi, E. Gaudry, J. Ledieu, V. Fournée, S. Alarcón Villaseca, J.-M. Dubois, Yu. Grin, P. Gille, W. Moritz, and R. D. Diehl, Phys. Rev. B **84**, 085411 (2011).
[9] R. D. Diehl, J. Ledieu, N. Ferralis, A. W. Szmodis, and R. McGrath, J. Phys.: Condens. Matter **15**, R63 (2003).
[10] Z. Papadopolos, P. Pleasants, G. Kasner, V. Fournée, C. J. Jenks, J. Ledieu, and R. McGrath, Phys. Rev. B **69**, 224201 (2004).
[11] B. Unal, C. J. Jenks, and P. A. Thiel, Phys. Rev. B **77**, 195419 (2008).
[12] M. Krajčí and J. Hafner, Phys. Rev. B **71**, 054202 (2005).
[13] M. Krajčí, J. Hafner, J. Ledieu, and R. McGrath, Phys. Rev. B **73**, 024202 (2006).
[14] M. Krajčí, J. Hafner, and M. Mihalkovič, Phys. Rev. B **73**, 134203 (2006).
[15] M. Krajčí and J. Hafner, Phys. Rev. B **84**, 115410 (2011).
[16] M. Krajčí and J. Hafner, Philos. Mag. **91**, 2904 (2011).
[17] M. Krajčí and J. Hafner, J. Catal. **278**, 200 (2011).
[18] M. Armbrüster, K. Kovnir, Yu. Grin, R. Schlögl, P. Gille, M. Heggen, M. Feuerbacher, European Patent EP09157875.7, 2009.
[19] M. Armbrüster, K. Kovnir, Yu. Grin, and R. Schlögl, in *Complex Metallic Alloys Fundamentals and Applications*, edited by J.-M. Dubois and E. Belin-Ferré (Wiley-VCH, Weinheim, 2010), pp. 385–399.
[20] J. Osswald, R. Giedigkeit, R. E. Jentoft, M. Armbrüster, F. Girgsdies, K. Kovnir, T. Ressler, Yu. Grin, and R. Schlögl, J. Catal. **258**, 210 (2008); J. Osswald, K. Kovnir, M. Armbrüster, R. Giedigkeit, R. E. Jentoft, U. Wild, Yu. Grin, and R. Schlögl, *ibid.* **258**, 219 (2008).
[21] K. Kovnir, M. Armbrüster, D. Teschner, T. V. Venkov, L. Szentmikosi, F. C. Jentoft, A. Knop-Gericke, Y. Grin, and R. Schlögl, Surf. Sci. **603**, 1784 (2009).
[22] M. Armbrüster, K. Kovnir, M. Behrens, D. Teschner, Y. Grin, and R. Schlögl, J. Am. Chem. Soc. **132**, 14745 (2010).
[23] M. Krajčí and J. Hafner, J. Phys. Chem. C **116**, 6307 (2012).
[24] M. Krajčí and J. Hafner, J. Catal. **295**, 70 (2012).
[25] D. Rosenthal, R. Widmer, R. Wagner, P. Gille, M. Armbrüster, Yu. Grin, R. Schlögl, and O. Gröning, Langmuir **28**, 6848 (2012).
[26] G. Kresse and J. Furthmüller, Phys. Rev. B **54**, 11169 (1996).
[27] G. Kresse and D. Joubert, Phys. Rev. B **59**, 1758 (1999).
[28] J. P. Perdew and Y. Wang, Phys. Rev. B **45**, 13244 (1992).
[29] P. Villars and L. D. Calvert, *Pearson's Handbook of Crystallographic Data for Intermetallic Phases* (American Society for Metals, Metals Park, OH, 1985).
[30] P. Gille, T. Ziemer, M. Schmidt, K. Kovnir, U. Burkhardt, and M. Armbrüster, Intermetallics **18**, 1663 (2010).
[31] L. Vočadlo, G. D. Price, and I. G. Wood, Acta Crystallogr. B **55**, 484 (1999).
[32] V. E. Dmitrienko, Acta Crystallogr. A **50**, 515 (1994).
[33] M. Krajčí, M. Windisch, J. Hafner, G. Kresse, and M. Mihalkovič, Phys. Rev. B **51**, 17355 (1995).
[34] See http://www.zometool.com.
[35] C. L. Henley, Phys. Rev. B **43**, 000993 (1991).
[36] M. Krajčí and J. Hafner, Phys. Rev. B **75**, 024116 (2007).
[37] Ö. Rapp and S. J. Poon, Phys. Rev. B **84**, 174206 (2011).
[38] V. Blum, L. Hammer, Ch. Schmidt, W. Meier, O. Wieckhorst, S. Müller, and K. Heinz, Phys. Rev. Lett. **89**, 266102 (2002).

[39]L. Hammer, V. Blum, Ch. Schmidt, O. Wieckhorst, W. Meier, S. Müller, and K. Heinz, Phys. Rev. B **71**, 075413 (2005).
[40]M. Finnis, Phys. Stat. Solidi A **166**, 397 (1998).
[41]K. Reuter and M. Scheffler, Phys. Rev. B **65**, 035406 (2001).
[42]J. Hafner and D. Spišák, Phys. Rev. B **75**, 195411 (2007).
[43]J. Prinz, R. Gaspari, C. A. Pignedoli, J. Vogt, P. Gille, M. Armbrüster, H. Brune, O. Gröning, D. Passerone, and R. Widmer, Angew. Chem. Int. Ed. **51**, 9339 (2012).
[44]G. Wulff, Z. Krystallogr. **34**, 445 (1901).
[45]F. Mittendorfer, N. Seriani, O. Dubay, and G. Kresse, Phys. Rev. B **76**, 233413 (2007).